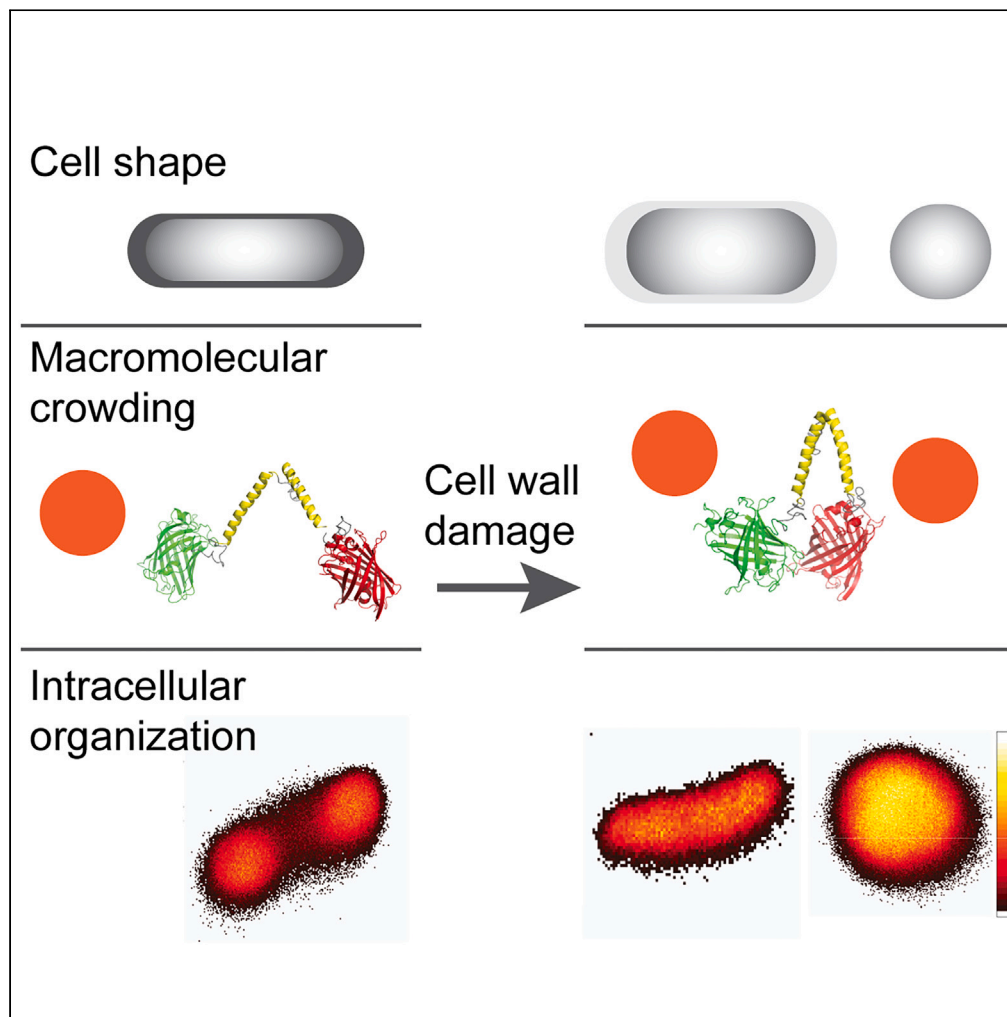**Article**

Cell wall damage increases macromolecular crowding effects in the *Escherichia coli* cytoplasm

Theodoros Pittas,
Weiyan Zuo,
Arnold J. Boersma

a.j.boersma@uu.nl

Highlights

Increased crowding effects in spheroplasts and penicillin-treated *Escherichia coli*

Crowding increase is not because of cell volume, shape, or protein synthesis

Cytoplasmic mixing and nucleoid expansion may explain increased crowding effects

iScience

Article

Cell wall damage increases macromolecular crowding effects in the *Escherichia coli* cytoplasm

Theodoros Pittas,[1,2] Weiyan Zuo,[1,2] and Arnold J. Boersma[1,3,4,*]

SUMMARY

The intracellular milieu is crowded with biomacromolecules. Macromolecular crowding changes the interactions, diffusion, and conformations of biomacromolecules. Changes in intracellular crowding have been mostly ascribed to differences in biomacromolecule concentration. However, spatial organization of these molecules should play a significant role in crowding effects. Here, we find that cell wall damage causes increased crowding effects in the *Escherichia coli* cytoplasm. Using a genetically encoded macromolecular crowding sensor, we see that crowding effects in spheroplasts and penicillin-treated cells well surpass crowding effects obtained using hyperosmotic stress. The crowding increase is not because of osmotic pressure, cell shape, or volume changes and therefore not crowder concentration. Instead, a genetically encoded nucleic acid stain and a DNA stain show cytoplasmic mixing and nucleoid expansion, which could cause these increased crowding effects. Our data demonstrate that cell wall damage alters the biochemical organization in the cytoplasm and induces significant conformational changes in a probe protein.

INTRODUCTION

The bacterial cytoplasm is a spatiotemporal continuum of dynamic interactions of macromolecules, which reflect its physicochemical properties. The total macromolecule concentration has been estimated at 300 mg/mL for *E. coli*.[1,2] A macromolecule in the cytoplasm that undergoes a conformational change, diffuses, or assembles with other bulky components is affected by the other macromolecules through steric repulsion and nonspecific chemical interactions.[3–6] Steric repulsion between the macromolecule and other macromolecules decreases the entropy of the system. This entropy can be increased by reducing the volume of the macromolecule(s). For a protein to compress, it needs an internal space where the crowders are excluded so that a (colloidal or osmotic) pressure difference can be built up, i.e., the depletion force. The nonspecific interactions are a sum of steric and chemical components and are weak at the single protein level but should become more pronounced at the ensemble level in a cell.

In vivo, crowding effects are complicated by the chemical and physical diversity of crowders and their heterogeneous distribution in the cell.[6,7] Cell components compartmentalize by demixing or preferential interactions in which protein crowders assemble with other biomolecules or membranes. Indeed, diffusion experiments have shown significant spatial heterogeneity in prokaryotes and eukaryotes.[8,9] Crowders captured in large complexes crowd less effectively because a crowder needs to diffuse to generate the depletion force, and complexation reduces the crowder number density. When crowders do not move, they will cause confinement effects, which are less pronounced until the confinement reaches the shape of a particular macromolecule. Hence, in the compartmentalized cell where biomolecules self-organize at various time and length scales to generate a heterogeneous cytoplasm, the effect of macromolecular crowding may not scale with bulk properties such as biopolymer volume fraction or protein density.

Cells exposed to stresses may see their crowding deviate from optimal levels. Crowding increases are observed when cell volume is reduced by osmotic stress or mechanical pressure, or increased biopolymer synthesis without a volume increase, as reported in some cases for eukaryotes.[10] In all these cases, it is the biopolymer concentration that changes. Crowding-sensitive probes allow the determination of these rapidly changing crowding effects. These probes are based on diffusion or protein conformation. The former measures viscosity which, among others, depends on the relative size of the tracer and crowders and is sensitive to large immobile obstacles such as a membrane.[9,11] Conformationally sensitive probes

[1]DWI-Leibniz Institute for Interactive Materials, Forckenbeckstrasse 50, 52074 Aachen, NRW, Germany

[2]Institute of Technical and Macromolecular Chemistry, RWTH Aachen University, Worringerweg 1, 52074 Aachen, NRW, Germany

[3]Cellular Protein Chemistry, Bijvoet Centre for Biomolecular Research, Faculty of Science, Utrecht University, Utrecht, the Netherlands

[4]Lead contact

*Correspondence: a.j.boersma@uu.nl

https://doi.org/10.1016/j.isci. 2023.106367

rely on compressing a probe protein.[12,13] A genetically encoded FRET-based probe for macromolecular crowding comprises a pair of two fluorescent proteins that form a FRET pair connected with a linker that facilitates compression in crowded environments, increasing FRET efficiency. The biosensor is sensitive to steric repulsion from crowders and has been applied in buffer, *E. coli*, yeast, and human cell lines in various conditions.[12,13] Careful choice of the fluorescent proteins allows addressing artifacts such as pH sensitivity or maturation, which is relevant under stress conditions.[14] This probe showed that crowding effects might deviate from the biopolymer volume fraction; osmotic stress-adapted cells have a lower effective crowding than expected from the biopolymer volume fraction.[15] In addition, energy depletion reduced crowding effects. Hence, most reported stresses that alter crowding do so through the biopolymer volume fraction while exceptions exist.

Cell wall damage is particularly harmful to cells, and many antibiotics act on cell walls. Complete or partial cell wall removal with β-lactam antibiotics such as the classical Penicillin G results in cell wall damage-induced dormancy or death in bacteria.[16–21] Penicillin inhibits murein-specific enzymes (penicillin-binding proteins) and disrupts cross-linking of the peptidoglycan in the cell wall.[16,22,23] Complete removal of the mechanical support leads to spherical cells named spheroplasts, or protoplasts. Spheroplasts can be generated with lysozyme- or Penicillin G[24–26] in a medium iso-osmolar with the cytoplasm to prevent lysis, or result from inhibiting cell shape-governing proteins.[27] The biopolymer volume fraction in spheroplasts has been determined. One study showed that these cells have the same biopolymer volume fraction as exponentially growing cells.[1] In contrast, other groups measured an increase in biomacromolecule content (DNA, RNA, and protein)[25,26,28–32]: Spheroplasts continue to synthesize molecules and can remain viable and regain their usual rod-like shape after spheroplasting.[25,33–35] Cell wall disruption can lead to a host of downstream effects. On one occasion, it was reported that cell wall damage with vancomycin reduced the diffusion of a DNA plasmid,[36] contrasting with various other types of antibiotics. Hence, although cell wall damage is a crucial mechanism for antibiotics, it is unclear whether it affects downstream crowding effects.

Here, using a FRET-based probe for macromolecular crowding, we demonstrate that partial or complete cell wall removal strongly increases macromolecular crowding effects. We see that the cytoplasm re-organizes where the nucleoid is less compartmentalized and increased mixing occurs. A better mixed cytoplasm may increase effective crowding.

RESULTS

Spheroplasting increases macromolecular crowding in *E. coli*

We first investigated the effect of spheroplasting in *E. coli* to determine the role of the cell wall on macromolecular crowding effects. We used two variants of our genetically encoded crowding sensor: the crGE and crGE2.3 (Figure 1A), which contain mCerulean3/mCitrine and mEGFP/mScarlet-I as FRET pairs, respectively. We quantified the FRET efficiency by dividing the FRET channel over the donor channel. The sensors are distributed homogeneously in the cytoplasm of exponentially growing cells and spheroplasts (Figure 1B). We generated spheroplasts using an EDTA-lysozyme-based protocol, which we name lysozyme-spheroplasts. Microscopy shows that some spheroplasts divide or bleb without cell wall, indicative of the L-form, which becomes more prevalent after 2h (Figure S1). We found that spheroplasts induce a substantially higher FRET ratio compared to exponentially growing cells (Figures 1C and 1D) for both the crGE from 0.93 ± 0.05 to 1.15 ± 0.018 ($\pm$s.d., n = 3) and the crGE2.3 probe from 0.15 ± 0.004 to 0.24 ± 0.04 ($\pm$s.d., n = 3). pH or maturation artifacts in the FRET ratio from the crGE are opposite to crGE2.3.[14,37] Therefore, a FRET increase in both sensors indicates a conformational change to a compressed state.

To assess the sensitivity to the external osmotic pressure, we returned the spheroplasts stepwise to the growth medium (MOPS minimal medium, ~220 mOsm) (Figure 1E). We see that the cells show an expected reduction in crowding to a ratio of 0.20 ± 0.01 ($\pm$s.d., n = 3), albeit this is still higher than cells with an intact cell wall at the same external osmolarity. The fluorescence from control cells (without transfected plasmid) was similarly low in exponentially growing cells and spheroplasts, thus excluding any autofluorescence-induced artifacts. We next verified that the crGE2.3 functions in *E. coli* as previously shown in yeast and buffer.[37] Indeed, we saw an increase in FRET ratio on a 500 mM NaCl osmotic upshift (~1 Osm) of exponentially growing cells from 0.15 ± 0.004 to 0.18 ± 0.02 ($\pm$s.d., n = 3). The ratio after osmotic upshift is lower than on spheroplast formation at ~0.8 Osm, indicating the drastic crowding change during spheroplasting (Figure 1E). Finally, we tested whether the increase was related to the lysozyme-based
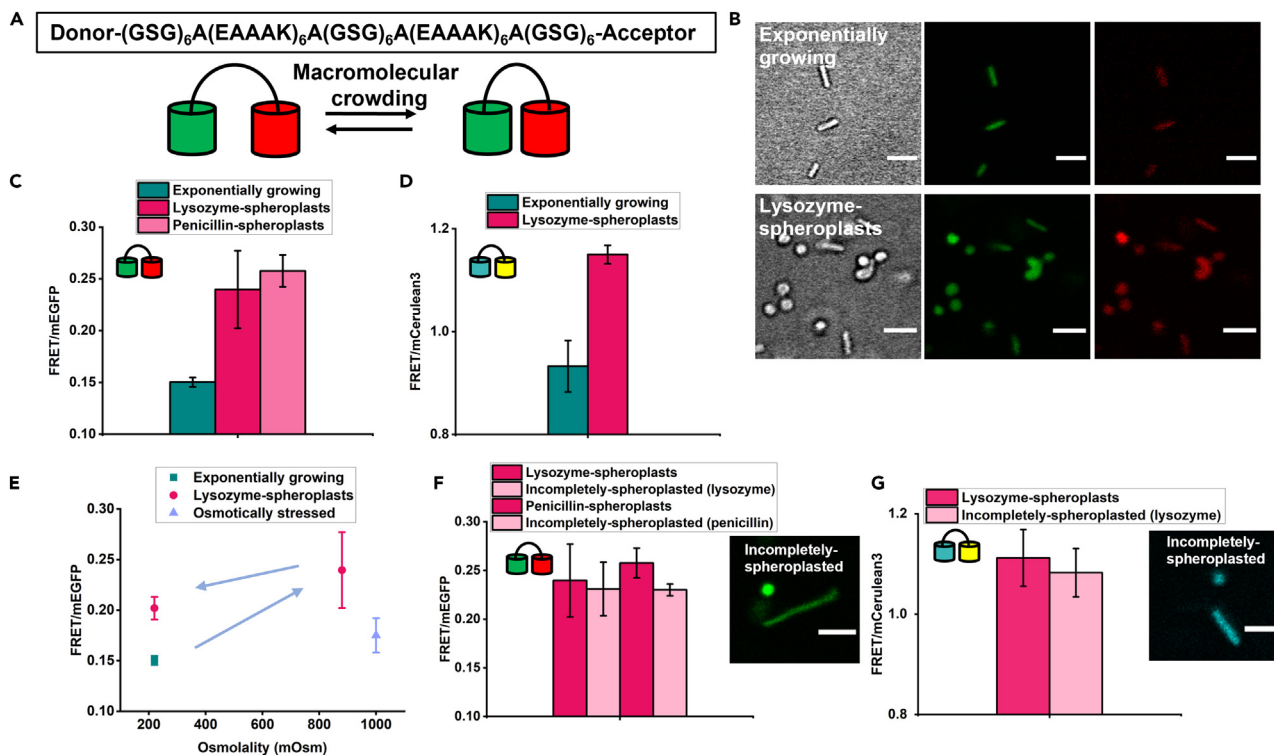
Figure 1. Spheroplast formation increases macromolecular crowding in *E. coli*

(A) The crGE2.3 (mEGFP/mScarlet-I) crowding sensor. Crowding reduces the distance between the acceptor and the donor, increasing the FRET efficiency.

(B) Representative confocal fluorescence microscopy images of exponentially growing cells and spheroplasts containing the crGE2.3 crowding sensor. Left panels is the brightfield, middle panels the donor emission, and right panel the acceptor emission on donor excitation.

(C) FRET/mEGFP emission ratio of exponentially growing cells and spheroplasts created either with Lysozyme- or Penicillin G-based protocols. See also Figure S2.

(D) FRET/mCerulean3 for crGE of exponentially growing cells and lysozyme-spheroplasts.

(E) The effect of osmolality on the crowding in spheroplasts. FRET/mEGFP of exponentially growing cells and osmotically stressed cells with 500 mM NaCl compared to the external osmolality of spheroplasts. Arrows is the order of treatment.

(F) Comparison of FRET/mEGFP in spheroplasts and rod-shaped cells remaining in the spheroplasting medium. Image depicts typical spherical and rod-shaped cells in the spheroplasting medium.

(G) As in (F) but with crGE. Error bars in C–G represent the standard deviation of the average FRET ratios of three independent biological replicates. The size of the scale bars is 4 μm.

spheroplasting protocol but observed similar FRET ratios when using Penicillin G instead of lysozyme (Figures 1C and S2), which we name penicillin-spheroplasts. These cells do not show any blebbing or division and are smaller, and growth and division capacity do therefore not play a role in crowding. Hence, spheroplasting increases macromolecular crowding effects.

Although the volume decrease of penicillin-spheroplasts (Figure 2E) would suggest that higher shrinkage induces a higher crowding, we find that incompletely spheroplasted cells that retain the rod shape give the same ratios as the fully spheroplasted cells (Figures 1F and 1G). This surprising result shows that cell volume, shape, and the mechanical constraints of the cell wall may not play a role in the spheroplast crowding increase.

Cell wall damage causes a macromolecular crowding increase

To verify whether cell wall damage without spheroplasting is sufficient to increase the macromolecular crowding as we see for incompletely spheroplasted cells, we treated exponentially growing cells with Penicillin G in MOPS medium (Figure 2A) without the osmotic upshift that stabilizes spheroplasts and monitored crowding in time. We chose the two sub-inhibitory concentrations of Penicillin G used in literature for spheroplasting[25] to treat our cells. We name these cells penicillin-treated cells. Although the pRSET-A plasmid encodes a beta-lactamase, we see that its activity is not sufficient to prevent the typical
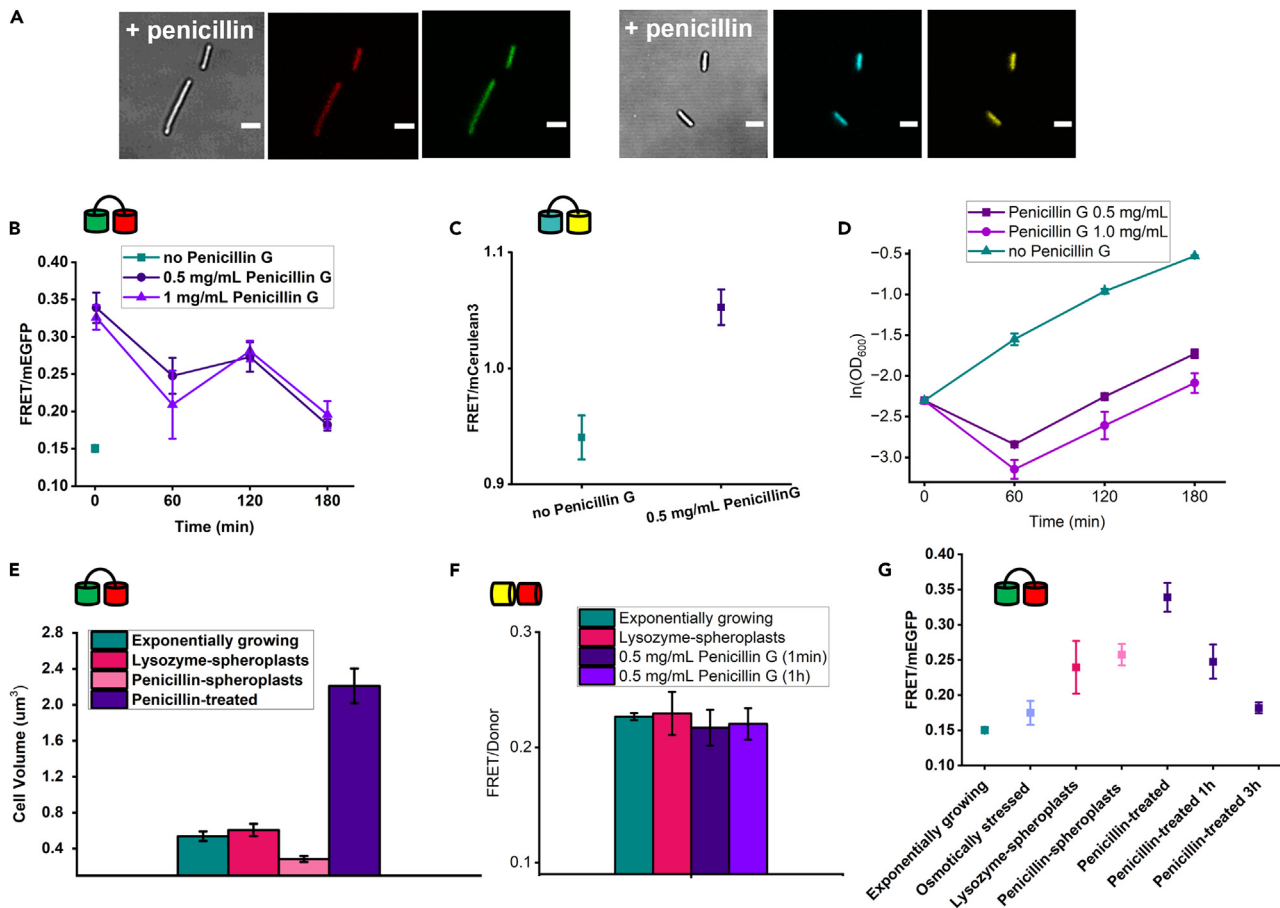
Figure 2. Penicillin G increases macromolecular crowding

(A) Fluorescence confocal microscopy images after penicillin treatment of *E. coli* BL21 with crGE3.2 (left three panels) and crGE (right three panels). Displayed are brightfield, donor, and acceptor channels after donor excitation.

(B) Time dependence of FRET/mEGFP treated with 0.5 or 1.0 mg/mL Penicillin G.

(C) FRET/mCerulean3 ratios for cells treated with 0.5 mg/mL Penicillin G for 1 min.

(D) Culture growth as optical density (OD_{600}) dependence on Penicillin G.

(E) Cell volume of exponentially growing cells, spheroplasts and Penicillin G-treated cells.

(F) FRET/mVenus ratios of the mVenus/mCherry construct in exponentially growing cells, spheroplasts, and Penicillin G-treated cells.

(G) Comparison of FRET ratio changes in various stress conditions. Error bars represent the standard deviation of the average of three independent biological replicates. The size of the scale bars is 4 μm.

effects of Penicillin G. We see that Penicillin G temporarily halted growth, and cell growth resumed 2 h after the treatment (Figure 2D). If stopping cell growth would result in a build-up of synthesized macromolecular crowders, the crowding should gradually increase. Unexpectedly, the FRET ratio increased within 1 min to 0.34 ± 0.02 (±s.d., n = 3) after adding 0.5 mg/mL Penicillin G (Figure 2B), which is higher than the spheroplasts. We tested the crGE probe, which also showed an immediate increase in FRET ratio to 1.05 ± 0.02 (±s.d., n = 3) (Figure 2C), which excludes pH effects. We see that the ratios remain high and decrease slowly over 3 h of adaptation in MOPS minimal medium containing Penicillin G to approach the FRET ratios of the spheroplasts. During the decrease in crowding effects, the OD increases slowly (Figure 2D). The changes in crowding are not owing to osmotic stress as the medium osmolarity remains similar with addition of Penicillin G (Table S1). To completely exclude optical or fluorescent protein artifacts in these stress conditions, we tested an mVenus-mCherry construct without a linker[38] to prevent intramolecular FRET changes. We found that the FRET ratios of spheroplasts and penicillin-treated cells are the same as exponentially growing cells (Figure 2F). Hence, the FRET increase is because of a compressed conformation of the crowding sensor, instantaneously induced by the action of Penicillin G on the cell wall.

The 1-min timeframe is too short for biopolymer synthesis to significantly increase crowding, considering that the cell maintains a 60-min doubling time. Therefore, we assessed whether the crowding increase is because of a decrease in cell volume. We determined the cell volume from fluorescent confocal microscopy images of the crGE2.3 probe that is evenly spread over the cytoplasm. For calculating cell volume, we considered rod-shaped cells as cylinders with hemi-spherical end caps and spheroplasts as spheres and used the half-maximum intensity to determine the width and the length of the cells (Figure S3). We find a cell volume of 0.54 ± 0.05 μm3 for exponentially growing cells, which is similar to lysozyme-spheroplasts (0.61 ± 0.07 μm3) but higher than penicillin-spheroplasts (0.29 ± 0.03 μm3) (Figure 2E). In contrast, cells that remained rod-shaped during spheroplasting have the same appearance as before spheroplasting. The diameter of our spheroplasts is similar to those found elsewhere.[39] In contrast, the volume of penicillin-treated cells without increasing the medium osmolarity increased steeply to 2.21 ± 0.19 μm3. Therefore, the cytoplasmic volume does not correspond to the crowding increase. The increase in FRET for both penicillin-treatment and spheroplasting shows that cell wall damage can be sufficient to increase crowding (Figure 2G).

Cytoplasmic mixing is a potential cause for the crowding increase

We next aimed to determine a potential cause for the crowding increase. Crowding effects depend not only on the absolute concentration of biomacromolecules or the biopolymer volume fraction in the entire cell but also on the macromolecular organization. For example, altering crowder distribution or their diffusion rate by complexation in weakly assembled large immobile complexes would generate less crowded areas where a sensor resides, and the effective crowding decreases. Moreover, a well-mixed cytoplasm would induce higher crowding as there are more collisions with crowders. The nucleoid forms a compartment in *E. coli* and is one of the main organizers of the cell: a compact nucleoid will take up less space, reducing the effect of protein-based crowders. Indeed, the nucleoid/cytoplasm ratio has been shown to affect cell biophysical properties strongly.[40] We therefore assessed the properties of the nucleoid to test the hypothesis that the macromolecular organization changes significantly on cell wall damage, which could increase crowding.

We first used a genetically encoded polynucleotide stain based on (KWK) repeat units fused to GFP to image the nucleoid.[41] We used a derivative based on two (KWK)$_2$ sequences for divalent binding. This probe has been shown to bind the nucleoid of *E. coli*, although these peptides also bind RNA *in vitro*.[42,43] We imaged the KWK probe localization by confocal fluorescence microscopy after 4-5 h expression with 100 μM IPTG. The probe is excluded from the cell poles in MOPS minimal medium and follows the location of the nucleoid (Figure S4). When we use LB medium, we see fluorescent foci in ∼70% of the cells (Figures 3A, S5, and S7), with the majority localizing at the poles. The poles are usually associated with the ribosomes and not the nucleoid, possibly becoming a binding partner at high expression levels in LB, which does not occur at lower KWK expression levels in MOPS. Upon spheroplasting, we see complete fluorescence mixing in the cytoplasm of MOPS and LB-grown cells, indicating a reduced organization and increased mixing (Figures S5–S7). In penicillin-treated cells, we see rapid dispersion of the KWK foci in about 75% of the population (Figures 3A, 3D, and S5–S7). After Penicillin G, the probe occupies the entire cell, including the pole regions. Incompletely spheroplasted cells showed a similar spread pattern to the penicillin-treated ones, thus indicating possible similarities between these two cellular states. Cells grown in MOPS medium did not have the foci that Penicillin G could disperse, and the probe remained dispersed (Figure S4). Hence, the genetically encoded polynucleotide-binding probe spreads throughout the cytoplasm upon cell wall damage.

To better map the consequences of cell wall damage, we stained the nucleoid selectively with DAPI. Exponentially growing cells can be grouped into three populations: those with two lobes, those with one mid-lobe, and those with a spread nucleoid (Figures 3B, 3C, 3E–3H, and S7). These likely correspond to the cell cycle stage: localization of DNA in two lobes is the characteristic pattern of the end of the replication cycle and beginning of division. In MOPS and LB, the two-lobed configuration is twice as prevalent as the other configurations. The similarity between MOPS and LB shows that the KWK foci in LB are not because of nucleoid staining but are more likely rRNA or mRNA staining. Within 1 min after the addition of Penicillin G, we see that the spread nucleoid state is twice as prevalent as the lobed states (Figures 3E and 3F). The nucleoid spreads throughout the entire cell, including the poles. The spread state is even more dominant after 1-h incubation with Penicillin G. These findings correspond to the dispersion of KWK foci and KWK spreading through the cytoplasm on the addition of Penicillin G. An increased mixing was also observed
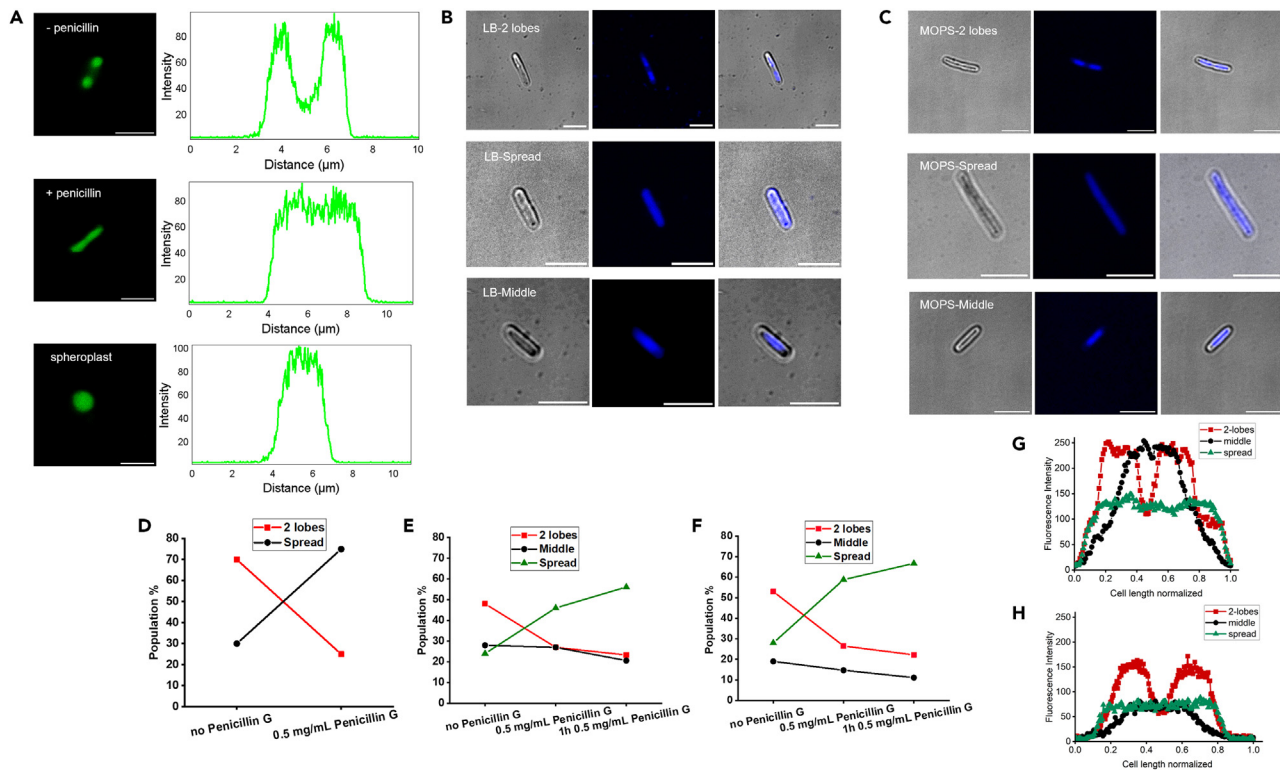
Figure 3. The nucleoid is more spread upon spheroplasting or penicillin treatment

(A) Fluorescence confocal microscopy images of *E. coli* BL21 expressing the KWK probe showing a difference in distribution in exponentially growing cells in LB medium, penicillin-treated cells (1 min after adding 0.5 mg/mL Penicillin G), and lysozyme-spheroplasts. Right panels are the corresponding fluorescence intensity over the longest axis in the bacteria.

(B) Fluorescence confocal microscopy images of DAPI-stained nucleoids in LB medium show three distinct categories.

(C) As in (B), cells were grown in MOPS medium.

(D) Increase in the percentage of cells with a spread nucleoid conformation upon Penicillin G addition.

(E) As in (D) where DAPI stain is used in LB medium, showing a similar pattern.

(F) As (E) with MOPS medium.

(G) DAPI fluorescence intensity along the longest axis of the bacteria for LB medium.

(H) As in (G) with MOPS medium. >35 cells per condition were analyzed. The size of the scale bars is 4 μm. See also Figures S5–S7.

in spheroplasts, where we used DRAQ5 dye to stain the nucleoid (Figure S8). Hence, cell wall damage homogenizes cytoplasmic content, as demonstrated by the nucleoid expansion and dispersion of an oligo-nucleotide-binding probe. These mixing effects offer a potential route to higher macromolecular crowding effects (Figure 4).

DISCUSSION

This study used a genetically encoded FRET biosensor to quantify macromolecular crowding effects in *E. coli* cells with a partly or fully removed cell wall. We find that (1) crowding effects in spheroplasts and penicillin-treated cells surpass the ones measured in osmotically stressed cells, (2) the observed effects are irrespective of cell shape, external osmolarity, biopolymer synthesis, and cell volume, and (3) cell wall damage possibly results in cytoplasmic homogenization and changes in nucleoid organization.

Our findings rely on sensors to measure macromolecular crowding. These sensors have been validated in different cell types, including during osmotic upshift in *E. coli*.[12,13] The sensors measure steric interactions, thus excluding interactions with proteins of the bacterial cytoplasm, whereas most other proteins would respond to additional nonsteric interactions under crowded conditions.[44,45] The sensors give information on the crowding effect at the 5–10 nm scale, which is in the FRET range. The sensors thus measure crowders or confinements in a similar size range, which is a typical size for an intracellular protein. The readout is not
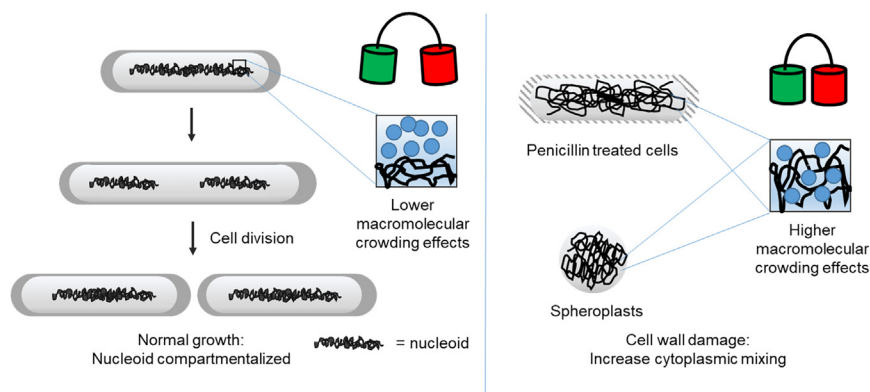
Figure 4. Schematic representation of nucleoid expansion with cell wall damage
Left panel: exponentially growing cells that divide and maintain a more compartmentalized cytoplasm. Right panel: partial (Penicillin G) or complete (spheroplasts) cell wall damage inhibits division and provides cells with a more expanded nucleoid. The more homogenized interior could lead to higher macromolecular crowding effects.

because of fluorescent protein effects. Therefore, beyond reasonable doubt, the sensor is highly compressed upon cell wall damage, showing drastic physiological changes. This compression is indicative of an effective macromolecular crowding increase at the size range of a typical protein.

Up to date, crowding effects have most frequently been correlated with volume changes and protein concentration.[1,10,13] Also, the crowding sensor reported crowding values corresponding to cell volume changes on osmotic stress. However, in previous work, we noticed that cells adapted to osmotic stress or energy depleted cells displayed reduced effective crowding, showing that crowding effects may not scale with the biopolymer volume fraction in the entire cytoplasm.[15] Here, we show the crowding can also greatly increase independent from the cell volume. In spheroplasts, the longer preparation time could in principle also increase crowding because of continued biopolymer synthesis that was measured before,[25,31] and in the case of penicillin-spheroplasts the cells are much smaller. However, the penicillin-treated cells and spheroplasts are linked by cell wall damage: even incompletely spheroplasted cells give the same results as penicillin-treated cells. The penicillin treated cells have a higher volume immediately after treatment, and therefore the concentration of macromolecules cannot increase but their crowding immediately after treatment is higher than spheroplasts. Therefore, additional biopolymer synthesis and cell volume effects may play a role, but this is not the main driver of the high crowding on cell wall damage.

The link between the cell wall and crowding that we see is not straightforward. The cell wall regulates the turgor pressure and maintains surface to mass ratio.[46] However, the short timeframe excludes a discrepancy between halted cell wall growth and cell volume and mass. On the other hand, many of the proteins involved in cell division are associated with cell wall maintenance and coordinate the segregation of DNA during cell division.[26,47,48] DNA is a prominent organizer in the cell, and its perturbation would have consequences on the physical-chemical properties of the cell. For example, under conditions that favor growth, the cytoplasm is a poor solvent for the nucleoid,[40] giving it its specific architecture and organization. In these conditions, DNA is withheld from the cell's end caps by entropic forces, whereas ribosomes and RNA species are more common in the end caps.[49] In healthy cells, DNA is dynamic, and replication begins in the mid-cell and in the intermediate stage of the cycle DNA molecules spread toward the poles. At the final stage of replication, the chromosome segregates in two lobes, and the two cells detach from each other.[47,50,51] Perturbation of these processes through the cell division machinery, improving the solvent quality of the cytoplasm, or altered transcription/translation may alter the DNA shape, conformation, and its mixing with the cytoplasm. We see in both spheroplasting and penicillin treatment that the nucleoid is expanded. These cell wall perturbations are highly suitable for our sensors because they do not stop transcription and translation, which would alter the fluorescence properties of our sensors by generating maturation artifacts.

How can the expansion of the nucleoid correlate with crowding changes? Of note is that the crowding increase is exceptionally high, much higher than the osmotic upshift, suggesting a dramatic

change in cytoplasmic material properties. Indeed, it has been shown that increased nucleoid size reduces the diffusion of larger particles.[40] Several explanations can be put forward in absence of a clear theory or relevant *in vitro* experiment. First, together with the expansion of the nucleoid into the poles, the high density of biopolymers at the poles (or other local densities)[52] mixes with the remainder of the cytoplasm. This mixing increases the crowder number density in the cytoplasm and the crowding effects. Moreover, it decreases less crowded spaces where the sensor would otherwise reside. Our KWK sensor shows that species that localized at the poles under normal growth conditions (like rRNA and mRNA) spread through the entire cell on spheroplasting or penicillin treatment, supporting this view.

The alternative hypothesis is that the nucleoid plays a causal role in increasing crowding by taking up more volume. The nucleoid is not a "classical" crowder that induces a colloidal osmotic pressure because of its large size: DNA would have an exceptionally low number density. In general, efficient crowders are somewhat smaller than the probe molecule,[7] so they have both high number density and sufficient volume. Instead, the nucleoid reduces the available space for the crowders compared to a compact and supercoiled nucleoid, thereby increasing their effective concentration, and crowding effects. We must note that the crowding readout is not exclusively a function of the nucleoid spreading because we see that during more prolonged exposure to penicillin, the nucleoid spreading increases somewhat but the crowding decreases (Figures 2B and 3F). This is not surprising in a living and adapting cell and it may be that its components start to self-organize. Next, other phenomena, such as RNA synthesis or collisions with the walls in confined spaces, may play a modulating role. DNA does not have specific interactions with the sensor as purified DNA at physiological concentration does not change its readout.[13]

A change in the macromolecular crowding and physicochemical properties of the bacterial cytoplasm may be a more common response to antibiotics: it was observed that vancomycin, also a cell wall inhibitor, decreases the motility of DNA and cytosol.[36] Moreover, nucleoid spreading is seen for other antibiotics, such as rifampicin and cecropin A, where nucleoid expands and mixes with ribosomes.[52–54] In addition, LL-37 also makes the nucleoid appear more diffuse, albeit this likely functions through crosslinking DNA.[55] Although these mechanisms may not be the same as described here and may not have the same effect at the protein scale, they induce large cytoplasmic changes and would alter crowding properties. This re-organization of biomolecules would have a plethora of downstream effects affecting biomolecule biogenesis, altering metabolic kinetics, and reducing cell growth, exacerbating the effect of the antibiotic.

Limitations of the study

Our work reveals increased crowding effects in wall-damaged bacteria, but the precise mechanism is yet to be determined. We do not know how cell wall damage leads to changes in DNA morphology. Elucidating whether DNA interacts with any cell wall components or how macromolecules such as ribosomes mix on cell wall damage would be useful in confirming our findings. In addition, it is unclear how the cytoplasmic organization changes crowding. We see DNA expansion and cytoplasmic mixing, which may account for the crowding increase by reducing less crowded regions. However, an alternative mechanism would be that DNA expansion excludes volume from the other crowding proteins and increase their effective concentration.

STAR★METHODS

Detailed methods are provided in the online version of this paper and include the following:

- KEY RESOURCES TABLE
- RESOURCE AVAILABILITY
  - Lead contact
  - Materials availability
  - Data and code availability
- EXPERIMENTAL MODELS AND SUBJECT DETAILS
- METHOD DETAILS
  - Growth conditions of *E. coli* cells
  - Osmotic stress experiments
  - Preparation of *E. coli* lysozyme-spheroplasts

- ○ Preparation of *E. coli* penicillin-spheroplasts
- ○ Penicillin-treated *E. coli*
- ○ KWK probe
- ○ Nucleoid staining
- ○ Microscopy settings & analysis
- ○ Cell volume calculations
- ● QUANTIFICATION AND STATISTICAL ANALYSIS

SUPPLEMENTAL INFORMATION

Supplemental information can be found online at https://doi.org/10.1016/j.isci.2023.106367.

AUTHOR CONTRIBUTIONS

P.T. and A.J.B. conceived the project. A.J.B. and P.T. designed the experiments and T.P. performed the experiments and analyzed the data. W.Z. designed and cloned the KWK sensor. T.P. and A.J.B. co-wrote the paper.

DECLARATION OF INTERESTS

The authors declare no competing interests.

REFERENCES

1. Zimmerman, S.B., and Trach, S.O. (1991). Estimation of macromolecule concentrations and excluded volume effects for the cytoplasm of Escherichia coli. J. Mol. Biol. *222*, 599–620. https://doi.org/10.1016/0022-2836(91)90499-V.

2. Cayley, S., Lewis, B.A., Guttman, H.J., and Record, M.T. (1991). Characterization of the cytoplasm of Escherichia coli K-12 as a function of external osmolarity: implications for protein-DNA interactions in vivo. J. Mol. Biol. *222*, 281–300. https://doi.org/10.1016/0022-2836(91)90212-O.

3. Zhou, H.-X., Rivas, G., and Minton, A.P. (2008). Macromolecular crowding and confinement: biochemical, biophysical, and potential physiological consequences. Annu. Rev. Biophys. *37*, 375–397. https://doi.org/10.1146/annurev.biophys.37.032807.125817.

4. Guin, D., and Gruebele, M. (2019). Weak chemical interactions that drive protein evolution: crowding, sticking, and quinary structure in folding and function. Chem. Rev. *119*, 10691–10717. https://doi.org/10.1021/acs.chemrev.8b00753.

5. Speer, S.L., Stewart, C.J., Sapir, L., Harries, D., and Pielak, G.J. (2022). Macromolecular crowding is more than hard-core repulsions. Annu. Rev. Biophys. *51*, 267–300. https://doi.org/10.1146/annurev-biophys-091321-071829.

6. van den Berg, J., Boersma, A.J., and Poolman, B. (2017). Microorganisms maintain crowding homeostasis. Nat. Rev. Microbiol. *15*, 309–318. https://doi.org/10.1038/nrmicro.2017.17.

7. Rivas, G., and Minton, A.P. (2022). Influence of nonspecific interactions on protein associations: implications for Biochemistry in vivo. Annu. Rev. Biochem. *91*, 321–351. https://doi.org/10.1146/annurev-biochem-040320-104151.

8. Garner, R.M., Molines, A.T., Theriot, J.A., and Chang, F. (2022). Vast heterogeneity in cytoplasmic diffusion rates revealed by nanorheology and Doppelgänger simulations. Preprint at bioRxiv. https://doi.org/10.1101/2022.05.11.491518.

9. Śmigiel, W.M., Mantovanelli, L., Linnik, D.S., Punter, M., Silberberg, J., Xiang, L., Xu, K., and Poolman, B. (2022). Protein diffusion in Escherichia coli cytoplasm scales with the mass of the complexes and is location dependent. Sci. Adv. *8*, eabo5387. https://doi.org/10.1126/sciadv.abo5387.

10. Neurohr, G.E., and Amon, A. (2020). Relevance and regulation of cell density. Trends Cell Biol. *30*, 213–225. https://doi.org/10.1016/j.tcb.2019.12.006.

11. Schavemaker, P.E., Śmigiel, W.M., and Poolman, B. (2017). Ribosome surface properties may impose limits on the nature of the cytoplasmic proteome. Elife *6*, e30084. https://doi.org/10.7554/eLife.30084.

12. Liu, B., Åberg, C., van Eerden, F.J., Marrink, S.J., Poolman, B., and Boersma, A.J. (2017). Design and properties of genetically encoded probes for sensing macromolecular crowding. Biophys. J. *112*, 1929–1939. https://doi.org/10.1016/j.bpj.2017.04.004.

13. Boersma, A.J., Zuhorn, I.S., and Poolman, B. (2015). A sensor for quantification of macromolecular crowding in living cells. Nat. Methods *12*, 227–229. https://doi.org/10.1038/nmeth.3257.

14. Liu, B., Mavrova, S.N., van den Berg, J., Kristensen, S.K., Mantovanelli, L., Veenhoff, L.M., Poolman, B., and Boersma, A.J. (2018). Influence of fluorescent protein maturation on FRET measurements in living cells. ACS Sens. *3*, 1735–1742. https://doi.org/10.1021/acssensors.8b00473.

15. Liu, B., Hasrat, Z., Poolman, B., and Boersma, A.J. (2019). Decreased effective macromolecular crowding in Escherichia coli adapted to hyperosmotic stress. J. Bacteriol. *201*, e00708-18. https://doi.org/10.1128/JB.00708-18.

16. Rogers, H.J. (1970). Bacterial growth and the cell envelope. Bacteriol. Rev. *34*, 194–214. https://doi.org/10.1128/br.34.2.194-214.1970.

17. Sailer, F.C., Meberg, B.M., and Young, K.D. (2003). β-Lactam induction of colanic acid gene expression in Escherichia coli. FEMS Microbiol. Lett. *226*, 245–249. https://doi.org/10.1016/S0378-1097(03)00616-5.

18. Ebel, W., Vaughn, G.J., Peters, H.K., and Trempy, J.E. (1997). Inactivation of mdoH leads to increased expression of colanic acid capsular polysaccharide in Escherichia coli. J. Bacteriol. *179*, 6858–6861. https://doi.org/10.1128/jb.179.21.6858-6861.1997.

19. Zeng, X., and Lin, J. (2013). Beta-lactamase induction and cell wall metabolism in Gram-negative bacteria. Front. Microbiol. *4*, 128.

20. Dörr, T., Alvarez, L., Delgado, F., Davis, B.M., Cava, F., and Waldor, M.K. (2016). A cell wall damage response mediated by a sensor kinase/response regulator pair enables beta-lactam tolerance. Proc. Natl. Acad. Sci. USA *113*, 404–409. https://doi.org/10.1073/pnas.1520333113.

21. Delhaye, A., Collet, J.-F., and Laloux, G. (2019). A fly on the wall: how stress response systems can sense and respond to damage to peptidoglycan. Front. Cell. Infect. Microbiol. *9*, 380.

22. Lee, M., Batuecas, M.T., Tomoshige, S., Domínguez-Gil, T., Mahasenan, K.V., Dik, D.A., Hesek, D., Millán, C., Usón, I., Lastochkin, E., et al. (2018). Exolytic and endolytic turnover of peptidoglycan by lytic transglycosylase Slt of Pseudomonas aeruginosa. Proc. Natl. Acad. Sci. USA *115*, 4393–4398. https://doi.org/10.1073/pnas.1801298115.

23. Cho, H., Uehara, T., and Bernhardt, T.G. (2014). Beta-lactam antibiotics induce a lethal malfunctioning of the bacterial cell wall synthesis machinery. Cell *159*, 1300–1311. https://doi.org/10.1016/j.cell.2014.11.017.

24. Renner, L.D., and Weibel, D.B. (2011). Cardiolipin microdomains localize to negatively curved regions of Escherichia coli membranes. Proc. Natl. Acad. Sci. USA *108*, 6264–6269. https://doi.org/10.1073/pnas.1015757108.

25. Hirokawa, H. (1962). Biochemical and cytological observations during the reversing process from spheroplasts to rod-form cells in escherichia coli. J. Bacteriol. *84*, 1161–1168. https://doi.org/10.1128/jb.84.6.1161-1168.1962.

26. Takahashi, S., and Nishida, H. (2017). Comparison of gene expression among normally divided cells, elongated cells, spheroplasts at the beginning of growth, and enlarged spheroplasts at 43h of growth in Lelliottia amnigena. Gene Rep. *7*, 87–90. https://doi.org/10.1016/j.genrep.2017.02.005.

27. Iwai, N., Nagai, K., and Wachi, M. (2002). Novel S-benzylisothiourea compound that induces spherical cells in Escherichia coli probably by acting on a rod-shape-determining protein(s) other than penicillin-binding protein 2. Biosci. Biotechnol. Biochem. *66*, 2658–2662. https://doi.org/10.1271/bbb.66.2658.

28. Kanazawa, H., and Wu, H.C. (1979). Lipoprotein synthesis in Escherichia coli spheroplasts: accumulation of lipoprotein in cytoplasmic membrane. J. Bacteriol. *137*, 818–823. https://doi.org/10.1128/jb.137.2.818-823.1979.

29. Tada, Y., and Yamaguchi, J. (1984). Characteristics of chromosomal DNA isolated from Escherichia coli spheroplasts. Microbiol. Immunol. *28*, 853–862. https://doi.org/10.1111/j.1348-0421.1984.tb00741.x.

30. Kuroda, T., Okuda, N., Saitoh, N., Hiyama, T., Terasaki, Y., Anazawa, H., Hirata, A., Mogi, T., Kusaka, I., Tsuchiya, T., et al. (1998). Patch clamp studies on ion pumps of the cytoplasmic membrane of Escherichia coli: formation, preparation, and utilization of giant vacuole-like structures consisting of everted cytoplasmic membrane. J. Biol. Chem. *273*, 16897–16904. https://doi.org/10.1074/jbc.273.27.16897.

31. Takahashi, S., and Nishida, H. (2015). Quantitative analysis of chromosomal and plasmid DNA during the growth of spheroplasts of *Escherichia coli*. J. Gen. Appl. Microbiol. *61*, 262–265. https://doi.org/10.2323/jgam.61.262.

32. Nishida, H. (2020). Factors that affect the enlargement of bacterial protoplasts and spheroplasts. Int. J. Mol. Sci. *21*, 7131. https://doi.org/10.3390/ijms21197131.

33. Jeynes, M.H. (1961). The growth and division of bacterial protoplasts. Exp. Cell Res. *24*, 255–264. https://doi.org/10.1016/0014-4827(61)90427-X.

34. Ranjit, D.K., and Young, K.D. (2013). The Rcs stress response and accessory envelope proteins are required for de novo generation of cell shape in Escherichia coli. J. Bacteriol. *195*, 2452–2462. https://doi.org/10.1128/JB.00160-13.

35. Weiss, D.S. (2013). Escherichia coli shapeshifters. J. Bacteriol. *195*, 2449–2451. https://doi.org/10.1128/JB.00306-13.

36. Wlodarski, M., Mancini, L., Raciti, B., Sclavi, B., Lagomarsino, M.C., and Cicuta, P. (2020). Cytosolic crowding drives the dynamics of both genome and cytosol in Escherichia coli challenged with sub-lethal antibiotic treatments. iScience *23*, 101560. https://doi.org/10.1016/j.isci.2020.101560.

37. Mouton, S.N., Thaller, D.J., Crane, M.M., Rempel, I.L., Terpstra, O.T., Steen, A., Kaeberlein, M., Lusk, C.P., Boersma, A.J., and Veenhoff, L.M. (2020). A physicochemical perspective of aging from single-cell analysis of pH, macromolecular and organellar crowding in yeast. Elife *9*, e54707. https://doi.org/10.7554/eLife.54707.

38. Wan, Q., Mouton, S.N., Veenhoff, L.M., and Boersma, A.J. (2022). A FRET-based method for monitoring structural transitions in protein self-organization. Cell Rep. Methods *2*, 100184. https://doi.org/10.1016/j.crmeth.2022.100184.

39. Figueroa, D.M., Wade, H.M., Montales, K.P., Elmore, D.E., and Darling, L.E. (2018). Production and visualization of bacterial

spheroplasts and protoplasts to characterize antimicrobial peptide localization. J. Vis. Exp. e57904. https://doi.org/10.3791/57904.

40. Xiang, Y., Surovtsev, I.V., Chang, Y., Govers, S.K., Parry, B.R., Liu, J., and Jacobs-Wagner, C. (2021). Interconnecting solvent quality, transcription, and chromosome folding in Escherichia coli. Cell *184*, 3626–3642.e14. https://doi.org/10.1016/j.cell.2021.05.037.

41. Lee, S., Oh, Y., Lee, J., Choe, S., Lim, S., Lee, H.S., Jo, K., and Schwartz, D.C. (2016). DNA binding fluorescent proteins for the direct visualization of large DNA molecules. Nucleic Acids Res. *44*, e6. https://doi.org/10.1093/nar/gkv834.

42. Mascotti, D.P., and Lohman, T.M. (1992). Thermodynamics of single-stranded RNA binding to oligolysines containing tryptophan. Biochemistry *31*, 8932–8946. https://doi.org/10.1021/bi00152a033.

43. Mascotti, D.P., and Lohman, T.M. (1993). Thermodynamics of single-stranded RNA and DNA interactions with oligolysines containing tryptophan. Effects of base composition. Biochemistry *32*, 10568–10579. https://doi.org/10.1021/bi00091a006.

44. Ebbinghaus, S., Dhar, A., McDonald, J.D., and Gruebele, M. (2010). Protein folding stability and dynamics imaged in a living cell. Nat. Methods *7*, 319–323. https://doi.org/10.1038/nmeth.1435.

45. Miklos, A.C., Sarkar, M., Wang, Y., and Pielak, G.J. (2011). Protein crowding tunes protein stability. J. Am. Chem. Soc. *133*, 7116–7120. https://doi.org/10.1021/ja200067p.

46. Oldewurtel, E.R., Kitahara, Y., and van Teeffelen, S. (2021). Robust surface-to-mass coupling and turgor-dependent cell width determine bacterial dry-mass density. Proc. Natl. Acad. Sci. USA *118*. e2021416118. https://doi.org/10.1073/pnas.2021416118.

47. Kleckner, N., Fisher, J.K., Stouf, M., White, M.A., Bates, D., and Witz, G. (2014). The bacterial nucleoid: nature, dynamics and sister segregation. Curr. Opin. Microbiol. *22*, 127–137. https://doi.org/10.1016/j.mib.2014.10.001.

48. Boes, A., Kerff, F., Herman, R., Touze, T., Breukink, E., and Terrak, M. (2020). The bacterial cell division protein fragment EFtsN binds to and activates the major peptidoglycan synthase PBP1b. J. Biol. Chem. *295*, 18256–18265. https://doi.org/10.1074/jbc.RA120.015951.

49. Mondal, J., Bratton, B.P., Li, Y., Yethiraj, A., and Weisshaar, J.C. (2011). Entropy-based mechanism of ribosome-nucleoid segregation in E. coli cells. Biophys. J. *100*, 2605–2613. https://doi.org/10.1016/j.bpj.2011.04.030.

50. Berlatzky, I.A., Rouvinski, A., and Ben-Yehuda, S. (2008). Spatial organization of a replicating bacterial chromosome. Proc. Natl. Acad. Sci. USA *105*, 14136–14140. https://doi.org/10.1073/pnas.0804982105.

51. Fisher, J.K., Bourniquel, A., Witz, G., Weiner, B., Prentiss, M., and Kleckner, N. (2013).

Four-dimensional imaging of E. coli nucleoid organization and dynamics in living cells. Cell *153*, 882–895. https://doi.org/10.1016/j.cell.2013.04.006.

52. Bakshi, S., Choi, H., Mondal, J., and Weisshaar, J.C. (2014). Time-dependent effects of transcription- and translation-halting drugs on the spatial distributions of the E. coli chromosome and ribosomes. Mol. Microbiol. *94*, 871–887. https://doi.org/10.1111/mmi.12805.

53. Bakshi, S., Choi, H., Rangarajan, N., Barns, K.J., Bratton, B.P., and Weisshaar, J.C. (2014). Nonperturbative imaging of nucleoid morphology in live bacterial cells during an antimicrobial peptide attack. Appl. Environ. Microbiol. *80*, 4977–4986. https://doi.org/10.1128/AEM.00989-14.

54. Zhu, Y., Weisshaar, J.C., and Mustafi, M. (2020). Long-term effects of the proline-rich antimicrobial peptide Oncocin112 on the Escherichia coli translation machinery. J. Biol. Chem. *295*, 13314–13325. https://doi.org/10.1074/jbc.RA120.013587.

55. Zhu, Y., Mohapatra, S., and Weisshaar, J.C. (2019). Rigidification of the Escherichia coli cytoplasm by the human antimicrobial peptide LL-37 revealed by superresolution fluorescence microscopy. Proc. Natl. Acad. Sci. USA *116*, 1017–1026. https://doi.org/10.1073/pnas.1814924116.

56. Schneider, C.A., Rasband, W.S., and Eliceiri, K.W. (2012). NIH Image to ImageJ: 25 years of image analysis. Nat. Methods *9*, 671–675. https://doi.org/10.1038/nmeth.2089.

57. Neidhardt, F.C., Bloch, P.L., and Smith, D.F. (1974). Culture medium for enterobacteria. J. Bacteriol. *119*, 736–747. https://doi.org/10.1128/jb.119.3.736-747.1974.

58. Rashid, F.-Z.M., Mahlandt, E., van der Vaart, M., Boer, D.E.C., Varela Alvarez, M., Henneman, B., Brocken, D.J.W., Voskamp, P., Blok, A.J., Shimizu, T.S., et al. (2022). HI-NESS: a family of genetically encoded DNA labels based on a bacterial nucleoid-associated protein. Nucleic Acids Res. *50*, e10. https://doi.org/10.1093/nar/gkab993.

STAR★METHODS

KEY RESOURCES TABLE

REAGENT or RESOURCE	SOURCE	IDENTIFIER
Bacterial and virus strains		
Escherichia coli BL21 (DE3)	Merck	#69450
Escherichia coli K12/DH5a	Thermo Fisher	#18265017
Chemicals, peptides, and recombinant proteins		
MOPS (3-(4-Morpholino) Propane Sulfonic Acid)	Sigma-Aldrich	CAS: 1132-61-2
Potassium phosphate dibasic	Sigma-Aldrich	CAS: 7758-11-4
Iron (II) Sulfate Heptahydrate	Sigma-Aldrich	CAS: 7782-63-0
Ammonium chloride	Sigma-Aldrich	CAS: 12125-02-9
Potassium sulfate	Sigma-Aldrich	CAS: 7778-80-5
Calcium chloride dihydrate	Sigma-Aldrich	CAS: 10035-04-8
Magnesium chloride hexahydrate	Sigma-Aldrich	CAS: 7791-18-6
Sodium chloride	Sigma-Aldrich	CAS: 7647-14-5
Ammonium molybdate (para)tetrahydrate	Sigma-Aldrich	CAS: 12054-85-2
Boric acid	Sigma-Aldrich	CAS: 10043-35-3
Copper sulfate pentahydrate	Sigma-Aldrich	CAS: 7758-99-8
Manganese sulfate monohydrate	Sigma-Aldrich	CAS: 10034-96-5
Zinc sulfate heptahydrate	Sigma-Aldrich	CAS: 7446-20-0
Cobalt(ii) chloride hexahydrate	Sigma-Aldrich	CAS: 7791-13-1
Ampicillin	TCI	CAS: 69-53-4
Sucrose	Sigma-Aldrich	CAS: 57-50-1
Lysozyme from chicken egg white	Sigma-Aldrich	CAS: 12650-88-3
DNAse I recombinant	Sigma-Aldrich	CAS: 9003-98-9
Ethylenediaminetetraacetic acid, EDTA	Sigma-Aldrich	CAS: 60-00-4
Sodium hydroxide	Sigma-Aldrich	CAS: 1310-73-2
Tris HCl	Sigma-Aldrich	CAS: 1185-53-1
Magnesium sulfate	Sigma-Aldrich	CAS: 7487-88-9
Penicillin G sodium salt	TIC	CAS: 69-57-8
LB Broth	Sigma-Aldrich	#L7025
LB Agar	Sigma-Aldrich	#L3147
D-(+)-Glucose	Sigma-Aldrich	CAS: 50-99-7
DAPI for nucleic acid staining	Sigma-Aldrich	CAS: 28718-90-3
DRAQ5 staining solution	Miltenyi Biotec	#130-117-344
Deposited data		
Analyzed data	This paper	https://zenodo.org/record/7653000#.Y_4Uzh_MJPY
Experimental models: Organisms/strains		
Escherichia coli BL21 (DE3)	Merck	#69450
Escherichia coli K12/DH5a	Thermo Fisher	#18265017
Recombinant DNA		
Plasmid: pRSET-A-KWK	ThermoFischer Scientific: GeneArt	N/A
Plasmid: pRSET-A-crGE2.3 (mEGFP/mScarlet-I)	ThermoFischer Scientific: GeneArt	N/A
Plasmid: pRSET-A-crGE (mCerulean3/mCitrine)	ThermoFischer Scientific: GeneArt	N/A

(Continued on next page)

Continued

REAGENT or RESOURCE	SOURCE	IDENTIFIER
Plasmid: pRSET-A-VC (mVenus-mCherry)	ThermoFischer Scientific: GeneArt	N/A
Software and algorithms		
ImageJ	Schneider et al., 2012[56]	https://imagej.nih.gov/ij/
Origin 2023	OriginLab Corporation	https://www.originlab.com/
Microsoft Office 2016 (Word, Excel)	Microsoft	https://www.microsoft.com/
Zotero	Open source	https://www.zotero.org/
Other		
Leica TCS SP8 confocal microscope	Leica	N/A
Incubator shaker	Eppendorf	S44i

RESOURCE AVAILABILITY

Lead contact

Further information and requests for resources and reagents should be directed to and will be fulfilled by the lead contact, Arnold J. Boersma (a.j.boersma@uu.nl).

Materials availability

DNA plasmids that are used in this study are made available from the lead contact.

Data and code availability

- Analysis data are publicly available through Zenodo and also listed in the key resources table (https://zenodo.org/record/7653000#.Y_4Uzh_MJPY). Microscopy images reported in this paper will be shared by the lead contact upon request.

- This paper does not report original code.

- Any additional information required to reanalyze the data reported in this paper is available from the lead contact upon request.

EXPERIMENTAL MODELS AND SUBJECT DETAILS

E. coli BL21 (DE3) cells were used in this study. The cells were cultured in MOPS minimal medium supplemented with glucose in a shaking incubator at 37°C.

METHOD DETAILS

Growth conditions of *E. coli* cells

We used *E. coli* BL21(DE3) for every experiment. The synthetic genes crGE2.3[37] and VC[38] in the plasmid pRSET-A were codon-optimized for *E. coli* and obtained from GeneArt. Bacteria were transformed with crGE2.3 (mEGFP-mScarlet-I) or the crGE (mCerulean3-mCitrine) crowding sensor.[13] A single colony of freshly transformed cells was picked and grown in overnight incubation in (5–6 mL) MOPS minimal medium[57] with 50 μg/mL ampicillin (TCI) at 37°C and 180 *rpm* agitation. The cell cultures were diluted to an OD600 of 0.03 in fresh MOPS (10 mL) at 100 mL Erlenmayer flasks and grown at 30°C and 180 *rpm* agitation until they reached an OD600 of 0.1–0.3. The sensor was expressed sufficiently without an inducer. Fluorescent cells were mixed with *E. coli* BL21 cells without plasmid of the same growth phase just before imaging. Experiments with spheroplasts, osmotic stress, and penicillin were conducted subsequently.

Osmotic stress experiments

For osmotic stress experiments we used 500 mM NaCl, as described also elsewhere.[13] Briefly, 1 mL of *E. coli* in the exponential growth phase was pelleted at 5000 *xrpm* for 5 min and re-suspended in MOPS medium supplemented with 500 mM NaCl, without any potassium sources or glucose, to avoid adaptation of the cells. The samples were immediately mounted on glass microscopy slides and imaged.

Preparation of *E. coli* lysozyme-spheroplasts

We created *E. coli* BL21 (DE3) spheroplasts following literature, with minor modifications.[24] 1 mL of the cell suspension in the exponential growth phase was pelleted at 3000 x*g* for 1 min. The pellet was re-suspended in 500 µL 0.8 M sucrose solution. Then we added the following solutions to the cell aliquots: 30 µL Tris-HCl (pH 8.0), 24 µL 0.5 mg/mL lysozyme, (~20 µg/mL final concentration), 6 µL 5 mg/mL DNase (~50 µg/mL final concentration), and 6 µL 125 mM EDTA-NaOH (pH 8.0) (~1.3 mM final concentration). Incubation of the sample for 10 min at 25 °C followed and 100 µL of STOP solution (10 mM Tris·HCl, pH 8, 0.7 M sucrose, 20 mM MgCl2) were added to terminate the digestion. The cell suspension was pelleted at 5000 x*rpm* for 5 min and re-suspended in 50–70 µL of the spheroplasting mixture containing the STOP solution. 15 µL of the sample were mounted on glass microscopy slides and the creation of *E. coli* spheroplasts was evaluated, using confocal laser scanning microscopy. For the adaptation of spheroplasts to a lower osmolarity medium, liquid cultures of spheroplasts were diluted to an osmolarity equal to our MOPS medium (220 mOsmol/kg), by addition of milliQ water.

Preparation of *E. coli* penicillin-spheroplasts

We created *E.coli* BL21 (DE3) spheroplasts as described elsewhere, with minor modifications.[25] Cell suspension in the exponential growth phase was pelleted at 5000 x*rpm* for 5 min and resuspended in 10% w/v sucrose solution. Then we added the following solutions: 0.5 mg/mL of sodium salt of Penicillin G and 0.2% w/v MgSO4. After ~1h incubation, 15 µl of cell suspension were mounted on a glass microscopy slide to evaluate the creation of *E. coli* spheroplasts.

Penicillin-treated *E. coli*

After the liquid cell cultures had reached the exponential growth phase, they were incubated in MOPS supplemented with 0.5 mg/mL or 1 mg/mL Penicillin G. We selected antibiotic concentrations that were previously used for creating bacterial spheroplasts.[25,33] Samples were collected immediately, 1h, 2h, and 3h after antibiotic treatment and pelleted at 5000 x*rpm* for 5 min and then 15 µL sample was mounted on glass microscopy slides for imaging.

KWK probe

The KWK probe was designed based on literature.[41] The gene was synthesized by W. Zuo and was cloned into the plasmid pRSET-A. *E. coli* BL21(DE3) containing the corresponding plasmid was grown in LB medium following the usual protocol. Protein synthesis was induced with 100 µM IPTG at an OD600 of 0.1 at 30°C for 5–6 h. The cells were mounted on a glass slide and were imaged.

Nucleoid staining

At an OD_{600} of 0.1 we added 10 µg/mL DAPI[58] or 10 µM DRAQ5 (final concentration) and allowed the cells to grow for ~ 2h. Then we created spheroplasts or treated cells with penicillin and used microscopy to evaluate nucleoid localization.

Microscopy settings & analysis

For imaging *E. coli* cells, glass microscopy slides were mounted on a Leica TCS SP8 laser-scanning confocal microscope. The crGE2.3 sensor was excited using a 488-nm Argon laser and the emission was split into a 500–550 nm and a 580–700 nm intensity channel. The mCerulean3-mCitrine crowding sensor was excited using a 405-nm LED laser, and the emission was split into a 465–505 nm channel and a 525–600 nm intensity channel. The KWK sensor was excited using a 488 nm Argon laser and the emission was set into a 510–550 nm channel. DAPI dye was excited using a 405-nm LED laser and the emission was split into a 430–550 nm channel. DRAQ5 dye was excited using a 510 nm Argon laser and the emission was set into a 600–700 nm channel.

Image analysis was performed with the use of ImageJ,[56] an open source scientific image processing program. We plotted the FRET channel intensity versus the Donor channel intensity for every FRET-based sensor and under all experimental conditions described in this work. The data were fitted in a linear equation using the least-squares approach and the slope as the average FRET ratio as described previously.[12]

Fluorescence intensity versus distance plots were made for straight, non-dividing cells using the plot profile option in ImageJ. Cell heat maps were made with Origin 2018b.

Cell volume calculations

To determine the volume, we approximated spheroplasts as spheres and rod-shaped cells as cylinders with hemispherical end caps. From the plot profile of the fluorescence intensity, we estimated the length and width of single rod-shaped cells. We used the half-maximum intensities to calculate the volumes. Then, we estimated the median volumes for each replicate (3 biological replicates in total) and then the average volume of the three medians. For spheroplasts, we selected cells in the fluorescence channel and measured the area by using the circle selection in ImageJ. The cell radius and volume were calculated from the area. Only fully spherical cells were chosen for analysis.

QUANTIFICATION AND STATISTICAL ANALYSIS

Unless noted otherwise, all reported values are the average of three independent biological replicates. The error bars are the standard deviation over these three replicates. The number of cells per measurement is listed in the Figure captions. Image analysis, quantification and statistical analysis tools are shown in the key resources table.